ISSN 1392-1207. MECHANIKA. Vol. 30, No. 2, 2024: 123–134

Vibration Analysis of Porous Functionally Graded Material Truncated Conical Shells in Axial Motion

Weiwei XIAO*, Siqi LIU, Xiaolin HUANG***, Xiaojun WU****, Xusheng YUAN*****

**School of Architecture and Transportation Engineering, Guilin University of Electronic Technology, Guilin 541004, Guangxi, China, E-mail: shawvivi@163.com*

***School of Architecture and Transportation Engineering, Guilin University of Electronic Technology, Guilin 541004, Guangxi, China, E-mail: 874637306@qq.com*

****School of Architecture and Transportation Engineering, Guilin University of Electronic Technology, Guilin 541004, Guangxi, China, E-mail: xlhuang@guet.edu.cn (Corresponding author)*

*****Primary Education College, Guangxi College for Preschool Education, Nanning 530022, Guangxi, China, E-mail: 43374732@qq.com*

******School of Architecture and Transportation Engineering, Guilin University of Electronic Technology, Guilin 541004, Guangxi, China, E-mail: 3150085054@qq.com*

https://doi.org/10.5755/j02.mech.34592

1. Introduction

Functionally graded material (FGM) truncated conical shells have been widely used in various engineering fields such as aerospace, transportation, and machinery. Studying the dynamic characteristics of these components has important theoretical significance and engineering value.

The stability problem of FGM components always attracts the attention of researchers [1-3], and many studies have been conducted on the vibration of functionally graded material truncated conical shells. Zhang et al.[4] analyzed the free vibration of FGM truncated conical shells under different boundary conditions using the generalized differential quadrature method based on Love's first approximation theory. The results showed that in addition to the material composition index, factors such as boundary conditions and geometric shape also have a significant impact on the fundamental frequency of FGM truncated conical shells. On the basis of classical thin shell theory, Sofiyev et al. [5-8] solved the dimensionless natural frequencies of free supported FGM conical shells and sandwich FGM conical shells using a more accurate first-order shear deformation theory. The numerical results showed that as the aspect ratio and half cone angle increased, the influence of transverse shear deformation on the frequency parameters of truncated conical shells decreased. H Abolhassanpouri et al. [9] analyzed the nonlinear vibration characteristics of axially moving homogeneous truncated conical shells using the Galerkin method based on the Von Kármán nonlinear model. The results showed that as the axial velocity increased, the maximum amplitude of the truncated conical shell first increased and then decreased, and the change in cone angle had a significant impact on the system response. Nezhadi et al. [10] studied the free and forced vibrations of FGM conical shells under four kinds of pulse loads based on first-order shear deformation theory. The results showed that for different cone angles, the natural frequencies of FGM conical shells first decreased and then increased with the increase of circumferential wave numbers, and the dynamic response of metal materials under step pulse load was the highest. V Mahesh [11] studied the effects of the auxetic core's rib-length ratio, inclination angle on the damped structural response using direct iterative method.

In practical engineering, due to the inadequacy of material preparation technology, some pores often appear in FGM during its production process. Rahmani et al. [12] analyzed the vibration characteristics of FGM sandwich truncated conical shells with two types of pore distribution under uniform, linear and nonlinear temperature distributions based on the improved higher-order sandwich shell theory. The results showed that in the lower power law index, the dimensional normalized fundamental frequency increased with the rise of the pore's volume fraction, and when the power law index increased to a certain value, the fundamental frequency decreased, and vice versa. References [13-20] studied the dynamic response and stability characteristics of FGM plates and shells containing pores under different conditions, and found that the influence of pores on various mechanical properties of the structure cannot be ignored.

At present, research on pore-containing components mainly focuses on plates and shells on elastic foundations, but there still are some research on components in axial motion. Hong M et al. [21] developed a reliable mathematical model to study dynamic and wave propagation characteristics in FGM axial bars at high frequencies. Shen et al.[22] investigated vibration and stability behaviors of functionally graded nanoplates with axial motion using Hamilton's principle and the Galerkin method. The results demonstrated that complex frequencies of the functionally graded nanoplate with axial motion decrease with an increase of axial velocity in the subcritical region. Yan T. et al. [23] analyzed the transverse vibration of a FGM traveling beam using Hamilton's principle and the direct multiscale method, and obtained the stability boundaries of subharmonic resonance and combination resonance. This study will focus on the vibration characteristics of axially moving porous FGM truncated conical shells. It is assumed that the FGM truncated cone shell concerned here is composed of two materials: metal and ceramic, and its pore volume cannot be ignored. The corresponding volume components is computed based on the mass components of metal and ceramic materials, and an improved mixing law model is used to calculate the FGM physical properties

parameters of uniform and non-uniform pore distribution. The effects of porosity, axial motion, and half cone angle on the free vibration and dynamic response of FGM truncated conical shells are explored to further understand the vibration characteristics of FGM truncated conical shells and provide a theoretical basis for promoting the application of FGM shells in related engineering.

2. Basic equations and solving methods

2.1. A FGM conical shell model

As shown in Fig. 1, the FGM truncated conical shell with pores is subjected to lateral dynamic loads $q(s, \theta, t)$ and moves axially at a uniform velocity V. L and h are the length and the thickness of it respectively. γ stands for the semi-vertex angle of the cone. R_1 and R_2 are the average radii of the small and large ends of the truncated shell. S_1 and S_2 represent the distance from vertex O to the small and large ends. A right-handed orthogonal curve coordinate system (s, θ, z) *is* used, where s is the coordinate of the generatrix direction with the cone top as the origin, θ is the coordinate in the circumferential direction, and z is the coordinate in the thickness direction ($-h/2 \le z \le h/2$). The internal pores of the truncated shell are assumed small and uniformly or non-uniformly distributed along the thickness direction, as shown in Fig. 2. Fig. 2, a shows uniformly distributed pores, and Fig. 2, b shows non-uniformly distributed. There are various types of non-uniform distribution of pores, and the type studied in this article is the common case where there are many pores in the middle and few pores at the top and bottom along the thickness direction of the shell [24].

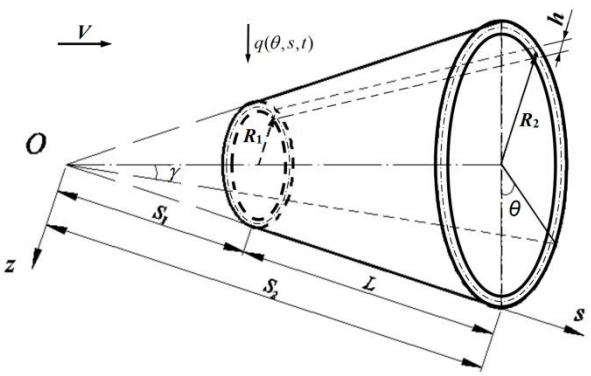

Fig. 1 FGM truncated conical shell with pores

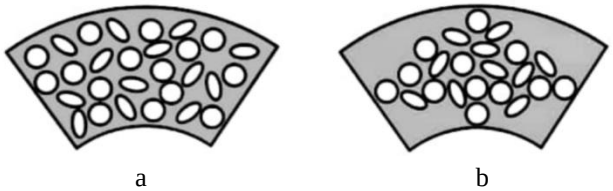

a b

Fig. 2 Distribution of pores along the thickness direction of the shell: a – uniformly distributed pores, b – non-uniformly distributed pores:

W_c and W_m respectively represent the mass fraction of ceramic and metal materials in the shell, and

$$W_c + W_m = 1. \tag{1}$$

The volume fraction of the two component materials and pores should meet:

$$V_c^* + V_m^* + \alpha^* = 1. \tag{2}$$

Here V_c^*, V_m^* and α^* represent the volume fractions of ceramics, metals, and pores in the entire truncated shell, respectively.

According to Eqs. (1) and (2), the volume fraction of ceramic V_c^* and metal materials V_m^* can be calculated as follows:

$$V_c^* = \left(1-\alpha^*\right)\frac{W_c/\rho_c}{W_c/\rho_c + W_m/\rho_m}, \tag{3a}$$

$$V_{\mathrm{m}}^* = \left(1-\alpha^*\right)\frac{W_{\mathrm{m}}/\rho_{\mathrm{m}}}{W_{\mathrm{c}}/\rho_{\mathrm{c}} + W_{\mathrm{m}}/\rho_{\mathrm{m}}}, \tag{3b}$$

where ρ_c and ρ_m are the densities of ceramic and metal, respectively.

The influence of internal pores on the mechanical properties of materials is very complex, and in addition to the distribution mode and position of pores, its size and shape also have an effect. This article focuses on micro pores, so the distribution pattern of pores and the total volume of pores are the main discussion objects. Two modes of pores' distribution are assumed along the thickness direction of the truncated conical shell, which are uniform and non-uniform. The porosity along the thickness direction of these two kinds of distribution are given as [15]:

$$\alpha(z) = \alpha^* \quad \text{(uniform)}, \tag{4}$$

$$\alpha(z) = \alpha^*\left(1-\frac{2|z|}{h}\right) \quad \text{(non-uniform)}. \tag{5}$$

Assuming that the volume fraction of ceramic materials V_c exhibits a power-law distribution along the thickness direction of the shell, then [15]:

$$V_c(z) = V_c^*\left(0.5 + z/h\right)^N, \ -h/2 \le z \le h/2, \tag{6}$$

where N is the volume composition index of the ceramic material $(0 \le N \le \infty)$.

According to the improved mixed law model, the effective material properties such as elastic modulus, density, and Poisson's ratio of FGM truncated conical shells with pores can be calculated as:

$$P_{eff} = P_c V_c + P_m\left(1-\alpha-V_c\right), \tag{7}$$

where P_c and P_m are the corresponding material properties of ceramics and metals, respectively.

Substituting Eqs. (4) and (6) into Eq. (7), the material properties of FGM truncated conical shells with uniformly distributed pores are obtained as:

$$P(z) = \left(P_c - P_m\right)V_c^*\left(0.5+\frac{z}{h}\right)^N + P_m\left(1-\alpha^*\right),$$
$$-h/2 \le z \le h/2. \tag{8}$$

Substituting Eqs. (5) and (6) into Eq. (7), non-uniform pore distribution FGM truncated conical shells' material properties are obtained as:

$$\begin{cases} P(z)=(P-P)V\left(0.5+\dfrac{z}{h}\right)+ \\ +P\left(1-\alpha\left(1-\dfrac{2z}{h}\right)\right),\ 0\le z\le h/2 \\ P(z)=(P-P)V\left(0.5+\dfrac{z}{h}\right)+ \\ +P\left(1-\alpha\left(1+\dfrac{2z}{h}\right)\right),\ -h/2\le z\le 0\,. \end{cases} \tag{9}$$

2.2. Governing equation and solution

Based on the classic thin shell deformation theory, the displacement field at any point of FGM truncated thin shells with pores can be expressed as [25]:

$$\begin{cases} \boldsymbol{u}=\boldsymbol{u_0}(\boldsymbol{s},\boldsymbol{\theta})-z\dfrac{\partial w}{\partial s} \\ \boldsymbol{v}=\boldsymbol{v_0}(\boldsymbol{s},\boldsymbol{\theta})-\dfrac{z}{s}\dfrac{\partial w}{\partial \varphi}, \\ \boldsymbol{w}=\boldsymbol{w}(\boldsymbol{s},\boldsymbol{\theta}) \end{cases} \tag{10}$$

where $\boldsymbol{u_0}$ and $\boldsymbol{v_0}$ are the mid-plane displacements along the direction $\boldsymbol{s}$ and $\boldsymbol{\theta}$ of the truncated shell, respectively.

The shells' strain component is described as [25]:

$$\{\boldsymbol{\varepsilon}\}=\begin{Bmatrix}\varepsilon_s\\ \varepsilon_\theta\\ \gamma_{s\theta}\end{Bmatrix}=\begin{Bmatrix}\varepsilon_s^0+z\kappa_s\\ \varepsilon_\theta^0+z\kappa_\theta\\ \gamma_{s\theta}^0+2z\kappa_{s\theta}\end{Bmatrix}, \tag{11}$$

where the mid plane strain $\boldsymbol{\varepsilon^0}$ and curvature $\boldsymbol{k}$ are respectively expressed as [25]:

$$\{\boldsymbol{\varepsilon^0}\}=\begin{Bmatrix}\varepsilon_s^0\\ \varepsilon_\theta^0\\ \gamma_{s\theta}^0\end{Bmatrix}=\begin{Bmatrix}\dfrac{\partial u}{\partial s}\\ \dfrac{1}{s}\dfrac{\partial v}{\partial \varphi}+\dfrac{u}{s}-\dfrac{w}{s}cot(\gamma)\\ \dfrac{1}{s}\dfrac{\partial u}{\partial \varphi}-\dfrac{v}{s}+\dfrac{\partial v}{\partial s}\end{Bmatrix}, \tag{12}$$

$$\{\boldsymbol{k}\}=\begin{Bmatrix}k_s\\ k_\theta\\ k_{s\theta}\end{Bmatrix}=-\begin{Bmatrix}\dfrac{\partial^2 w}{\partial s^2}\\ \dfrac{1}{s^2}\dfrac{\partial^2 w}{\partial \varphi^2}+\dfrac{1}{s}\dfrac{\partial w}{\partial s}\\ \dfrac{1}{s}\dfrac{\partial^2 w}{\partial s\partial \varphi}-\dfrac{1}{s^2}\dfrac{\partial w}{\partial \varphi}\end{Bmatrix}. \tag{13}$$

According to the constitutive relationship between stress and strain, the internal forces $\{\boldsymbol{N}\}=[N_s,\ N_\theta,\ N_{s\theta}]^T$, $\{\boldsymbol{M}\}=[M_s,\ M_\theta,\ M_{s\theta}]^T$ are given as:

$$\begin{Bmatrix}\boldsymbol{N}\\ \boldsymbol{M}\end{Bmatrix}=\begin{bmatrix}A & B\\ B & D\end{bmatrix}\begin{Bmatrix}\boldsymbol{\varepsilon}^0\\ \boldsymbol{k}\end{Bmatrix}, \tag{14}$$

where the elements A_{ij}, B_{ij}, D_{ij} of the stiffness matrices A, B, and D are defined as:

$$(A_{ij},B_{ij},D_{ij})=\int_{-h/2}^{h/2}Q_{ij}(1,z,z^2)dz\quad (i,j=1,2,6). \tag{15}$$

The $Q_{ij}(1, 2, 6)$ above is the conversion elastic constant of the shell, and defined as:

$$\begin{cases} Q_{11}=Q_{22}=\dfrac{E(z)}{1-\nu^2} \\ Q_{12}=Q_{21}=\dfrac{\nu E(z)}{1-\nu^2} \\ Q_{66}=\dfrac{E(z)}{2(1+\nu)} \\ Q_{16}=Q_{61}=Q_{26}=Q_{62}=0\,. \end{cases} \tag{16}$$

The first equation of Eq. (14) can be transformed into

$$\begin{cases} \varepsilon_\theta^0=A_{11}^*N_\theta+A_{12}^*N_s+B_{11}^*\kappa_s+B_{12}^*\kappa_\theta \\ \varepsilon_s^0=A_{21}^*N_\theta+A_{22}^*N_s+B_{21}^*\kappa_s+B_{22}^*\kappa_\theta\,. \\ \gamma_{s\theta}^0=A_{66}^*N_{s\theta}+B_{66}^*\kappa_{s\theta} \end{cases} \tag{17}$$

The constants $A_{ij}^*(1, 2, 6)$ and $B_{ij}^*(1, 2, 6)$ are shown in Appendix A.

$$\begin{cases} M_s=C_{11}^*N_\theta+C_{12}^*N_s+D_{11}^*\kappa_s+D_{12}^*\kappa_\theta \\ M_\theta=C_{21}^*N_\theta+C_{22}^*N_s+D_{21}^*\kappa_s+D_{22}^*\kappa_\theta\,. \\ M_{s\theta}=C_{66}^*N_{s\theta}+D_{66}^*\kappa_{s\theta} \end{cases} \tag{18}$$

The constants $C_{ij}^*(1, 2, 6)$ and $D_{ij}^*(1, 2, 6)$ are shown in Appendix B.

Based on the Hamiltonian variational principle, the dynamic equilibrium equation of porous FGM truncated conical shells in axial motion can be derived as [15, 22]:

$$\begin{cases} s\dfrac{\partial N_s}{\partial s}+\dfrac{\partial N_{s\theta}}{\partial \varphi}+N_s-N_\theta=I_0\dfrac{\partial^2 u_0}{\partial t^2} \\ \dfrac{\partial N_\theta}{\partial \varphi}+s\dfrac{\partial N_{s\theta}}{\partial s}+2N_{s\theta}=I_0\dfrac{\partial^2 v_0}{\partial t^2} \\ \dfrac{\partial^2 M_s}{\partial s^2}+\dfrac{2}{s}\dfrac{\partial M_s}{\partial s}+\dfrac{2}{s}\left(\dfrac{\partial^2 M_{s\theta}}{\partial s\partial \varphi}+\dfrac{1}{s}\dfrac{\partial M_{s\theta}}{\partial \varphi}\right)+\dfrac{1}{s^2}\dfrac{\partial^2 M_\theta}{\partial \varphi^2}-\dfrac{1}{s}\dfrac{\partial M_\theta}{\partial s}-\dfrac{N_\theta}{s}cot(\gamma)=I_0\left(\dfrac{\partial^2 w}{\partial t^2}+2V\dfrac{\partial^2 w}{\partial s\partial t}+V^2\dfrac{\partial^2 w}{\partial s^2}\right), \end{cases} \tag{19}$$

where I_0 is the mass coefficient along the thickness direction, and defined as $I_0 = \int_{-h/2}^{h/2} \rho(z)dz$.

The stress function F is introduced, and the relationship between F and the internal force in the shell is given as:

$$\begin{cases} N_s = \dfrac{1}{s^2}\dfrac{\partial^2 F}{\partial \varphi^2} + \dfrac{1}{s}\dfrac{\partial F}{\partial s}, N_\theta = \dfrac{\partial^2 F}{\partial s^2}, \\ N_{s\theta} = -\dfrac{1}{s}\dfrac{\partial^2 F}{\partial s \partial \varphi} + \dfrac{1}{s^2}\dfrac{\partial F}{\partial \varphi} \end{cases}, \tag{20}$$

here N_s and N_θ are the tensile (compressive) forces in the direction of s and θ respectively, and $N_{s\theta}$ is the shear force.

The deformation compatibility equation for truncated conical shells can be written as:

$$\frac{\cot(\gamma)}{s}\frac{\partial^2 w}{\partial s^2} - \frac{1}{s}\frac{\partial^2 \gamma_{s\theta}^0}{\partial s \partial \varphi} - \frac{1}{s^2}\frac{\partial \gamma_{s\theta}^0}{\partial \varphi} + \frac{\partial^2 \varepsilon_\theta^0}{\partial s^2} + \frac{1}{s^2}\frac{\partial^2 \varepsilon_s^0}{\partial \varphi^2} + \frac{2}{s}\frac{\partial \varepsilon_\theta^0}{\partial s} - \frac{1}{s}\frac{\partial \varepsilon_s^0}{\partial s} = 0. \tag{21}$$

To convert variable coefficient differential Eqs. (20) and (21) into constant coefficient differential equations, the following variable substitutions are introduced:

$$s = S_1 e^x, F = F_1 e^{2x}. \tag{22}$$

Substituting Eqs. (17), (18), (20), and (22) into Eqs. (19) and (21), the dynamic control equation for axially moving porous FGM truncated conical shells under lateral dynamic loads $q(s, \theta, t)$ can be derived as:

$$\begin{aligned} &\frac{-2\cot(\gamma)}{S_1^2}F_1 + \left[\frac{-3e^x}{S_1^2}\cot(\gamma) + g_{111}\right]\frac{1}{e^x}\frac{\partial F_1}{\partial x} + \left[\frac{-e^x}{S_1^2}\cot(\gamma) + g_{112}\right]\frac{1}{e^x}\frac{\partial^2 F_1}{\partial x^2} + g_{113}\frac{1}{e^x}\frac{\partial^3 F_1}{\partial x^3} + \\ &+ g_{114}\frac{1}{e^x}\frac{\partial^4 F_1}{\partial x^4} + g_{115}\frac{1}{e^x}\frac{\partial^2 F_1}{\partial \varphi^2} + g_{116}\frac{1}{e^x}\frac{\partial^3 F_1}{\partial x \partial \varphi^2} + g_{117}\frac{1}{e^x}\frac{\partial^4 F_1}{\partial x^2 \partial \varphi^2} + g_{118}\frac{1}{e^x}\frac{\partial^4 F_1}{\partial \varphi^4} + \\ &+ g_{121}\frac{1}{e^{3x}}\frac{\partial w}{\partial x} + g_{122}\frac{1}{e^{3x}}\frac{\partial^2 w}{\partial x^2} + g_{123}\frac{1}{e^{3x}}\frac{\partial^3 w}{\partial x^3} + g_{124}\frac{1}{e^{3x}}\frac{\partial^4 w}{\partial x^4} + g_{125}\frac{1}{e^{3x}}\frac{\partial^2 w}{\partial \varphi^2} + g_{126}\frac{1}{e^{3x}}\frac{\partial^3 w}{\partial x \partial \varphi^2} + \\ &+ g_{127}\frac{1}{e^{3x}}\frac{\partial^4 w}{\partial x^2 \partial \varphi^2} + g_{128}\frac{1}{e^{3x}}\frac{\partial^4 w}{\partial \varphi^4} + S_1 e^x q - S_1^4 e^{2x} I_0\left(\frac{\partial^2 w}{\partial t^2} + \frac{2V}{S_1 e^x}\frac{\partial^2 w}{\partial x \partial t} + \frac{V^2}{S_1^2 e^{2x}}\frac{\partial^2 w}{\partial x^2}\right) = 0, \end{aligned} \tag{23}$$

$$\begin{aligned} &\frac{g_{211}}{e^{2x}}\frac{\partial F_1}{\partial x} + \frac{g_{212}}{e^{2x}}\frac{\partial^2 F_1}{\partial x^2} + \frac{g_{213}}{e^{2x}}\frac{\partial^3 F_1}{\partial x^3} + \frac{g_{214}}{e^{2x}}\frac{\partial^4 F_1}{\partial x^4} + \frac{g_{215}}{e^{2x}}\frac{\partial^2 F_1}{\partial \varphi^2} + \frac{g_{216}}{e^{2x}}\frac{\partial^4 F_1}{\partial \varphi^4} + \\ &+ \frac{g_{217}}{e^{2x}}\frac{\partial^3 F_1}{\partial x \partial \varphi^2} + \frac{g_{218}}{e^{2x}}\frac{\partial^4 F_1}{\partial x^2 \partial \varphi^2} + \left(\frac{-e^x}{S_1^3}\cot(\gamma) + g_{221}\right)\frac{1}{e^{4x}}\frac{\partial w}{\partial x} + \left(\frac{e^x}{S_1^3}\cot(\gamma) + g_{222}\right)\frac{1}{e^{4x}}\frac{\partial^2 w}{\partial x^2} + \\ &+ \frac{g_{223}}{e^{4x}}\frac{\partial^3 w}{\partial x^3} + \frac{g_{224}}{e^{4x}}\frac{\partial^4 w}{\partial x^4} + \frac{g_{225}}{e^{4x}}\frac{\partial^2 w}{\partial \varphi^2} + \frac{g_{226}}{e^{4x}}\frac{\partial^4 w}{\partial \varphi^4} + \frac{g_{227}}{e^{4x}}\frac{\partial^3 w}{\partial x \partial \varphi^2} + \frac{g_{228}}{e^{4x}}\frac{\partial^4 w}{\partial x^2 \partial \varphi^2} = 0. \end{aligned} \tag{24}$$

Parameters $g_{ijk}(i, j, k = 1, 2, 3\ldots)$ are shown in Appendix C.

In the present case, the small and large ends of the shell are assumed to be simply supported. The boundary conditions are stated as:

$$v = w = M_s = 0, \text{ at } S = S_1, S_2. \tag{25}$$

So, the solution of Eqs. (23) and (24) is sought in the following form as [25]:

$$\boldsymbol{w}(x,\varphi,t) = \sum_{m_1}^{\infty}\sum_{n_1}^{\infty} w_{m_1 n_1}(t) e^x \sin(m_1 x)\sin(n_1 \varphi), \tag{26}$$

where $w_{m_1 n_1}(t)$ is the undetermined function, $m_1 = m\pi/x_0$, $x_0 = ln(S_2/S_1)$, m is the half wave number along the generatrix direction and n is the full wave number along the circumference direction.

Substituting Eq. (26) into Eq. (24) and using the harmonic balance method to obtain $\boldsymbol{F_1}(x, \varphi, t)$.

$$F_1(x,\varphi,t) = \sum_{m_1}^{\infty}\sum_{n_1}^{\infty} w_{m_1 n_1}(t)\begin{bmatrix} K_1 e^{-x}\sin(m_1 x) + \\ +K_2 e^{-x}\cos(m_1 x) + \\ +K_3\cos(m_1 x) + \\ +K_4\sin(m_1 x) \end{bmatrix}\sin(n_1 \varphi). \tag{27}$$

The coefficient K_i is defined as:

$$\begin{cases} K_1 = \dfrac{-(a_{11}a_{13} + a_{12}a_{14})}{a_{11}^2 + a_{12}^2} \\ K_2 = \dfrac{(a_{11}a_{14} - a_{12}a_{13})}{a_{11}^2 + a_{12}^2} \\ K_3 = \dfrac{(a_{21}a_{24} - a_{22}a_{23})}{a_{21}^2 + a_{22}^2} \\ K_4 = \dfrac{-(a_{21}a_{23} + a_{22}a_{24})}{a_{21}^2 + a_{22}^2} \end{cases}, \tag{28}$$

where the parameters a_{ij} $(i, j = 1, 2...)$ are shown in Appendix D [26].

Substituting Eqs. (26) and (27) into the dynamic equilibrium Eq. (23), multiplying $e^x sin(m_1 x) sin(n_1 \varphi)$ with both sides of Eq. (23) and conducting Galerkin integration in the shell domain, the second order linear ordinary differential equation about $w_{m_1 n_1}(t)$ is obtained as follows.

$$\boldsymbol{M}_{\boldsymbol{m_1 n_1}} \frac{d^2 w_{m_1 n_1}(t)}{dt^2} + \boldsymbol{C}_{\boldsymbol{m_1 n_1}} \frac{dw_{m_1 n_1}(t)}{dt} + \\ + \boldsymbol{K}_{\boldsymbol{m_1 n_1}} w_{m_1 n_1}(t) = q_{m_1 n_1}(t). \quad (29)$$

Where:

$q_{m_1 n_1}(t) = \int_0^{x_0} \int_0^{2\pi \sin(\gamma)} q(x,\varphi,t) e^x \sin(m_1 x) \sin(n_1 \varphi) d\varphi dx$, and $M_{m_1 n_1}$, $C_{m_1 n_1}$, $K_{m_1 n_1}$ are the generalized mass, damping coefficient, and stiffness coefficient of the shell, respectively.

When $q(x, \varphi, t) = 0$, Eq. (29) is the damped free vibration equation of an axially moving truncated conical shell containing porous functionally graded materials. Giving and $w_{m_1 n_1}(t) = a e^{\bar{\omega}_{m_1 n_1} t}$ substituting it into Eq. (29). Since a is not zero, to have a non-zero solution to the equation, there must be

$$det\left(\bar{\omega}_{m_1 n_1}^2 \boldsymbol{M}_{\boldsymbol{m_1 n_1}} + \bar{\omega}_{m_1 n_1} \boldsymbol{C}_{\boldsymbol{m_1 n_1}} + \boldsymbol{K}_{\boldsymbol{m_1 n_1}}\right) = 0 . \quad (30)$$

From the above equation, the free vibration frequency $\bar{\omega}_{m_1 n_1}$ of (m, n) mode can be obtained.

When solving forced vibration problems, the lateral dynamic load can be expressed as $q(x, \varphi, t) = q_0 f_1(x, \varphi) f_2(t)$, where q_0 is the load concentration, $f_1(x, \varphi)$ is the distribution function, $f_2(t)$ is the time variation function, and the time variation function of sudden load application is described as:

$$f_2(t) = \begin{cases} 0, & t = 0 \\ 1, & t > 0 \end{cases} . \quad (31)$$

When $f_2(t)$ is an arbitrary function, the dynamic response can be directly solved using the Duhamel's integral.

3. Example comparison and parameter analysis

3.1. Example Comparison

The dimensionless natural frequencies of isotropic truncated conical shells in axial motion under the condition of simple support on both sides are calculated in this present study, and the results are compared with the reference [9], taking modes $m = 1$ and $n = 6$. The results are shown in Fig 3. The computation data of the homogeneous truncated conical shells involving are material Young's modulus $E = 201.04$ GPa, density $\rho = 8.166$ kg/cm^3, semi-vertex angle $\gamma = \pi/6$, thickness $h = 0.004$ m, diameter to thickness ratio $R_2/h = 100$, length $L = 0.25 S_2$. The dimensionless natural frequency is defined as $f = \bar{\omega} R_2 \sqrt{\rho(1-\nu^2)/E}$.

As shown in the Fig. 3, a good agreement is obtained with a maximum relative error of 2.84%.

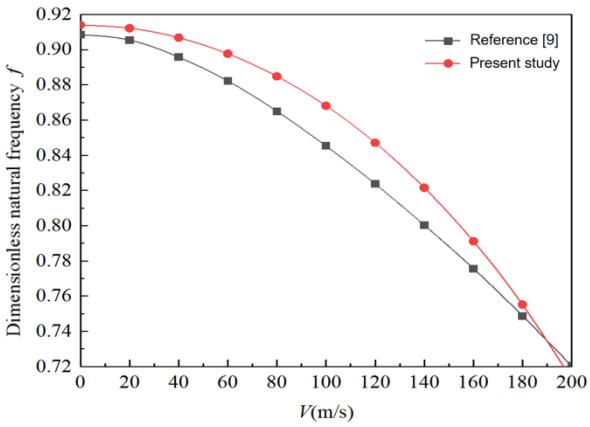

Fig. 3 The variation of the natural frequency f of an axial moving isotropic truncated conical shell versus velocity V

3.2. Parameter analysis

The effects of factors such as material composition index, axial motion velocity, ceramic material mass fraction, porosity, pore type, and geometric parameters of truncated conical shells on the free vibration and dynamic response of axially moving porous FGM truncated conical shells are analyzed in this subsection. The FGM truncated cone shell materials are metal SUS304 and ceramic Si3N4, with physical properties parameters of $E_m = 201.4$ GPa, $\rho_m = 8.166$ g/cm^3, $\nu_m = 0.3262$; $E_c = 348.43$ GPa, $\rho_c = 2.37$ g/cm^3, $\nu_c = 0.24$.

3.2.1. Free vibration

Dimensionless natural frequency f defined above, taking modes $m = 1$ and $n = 6$. FGM truncated shell thickness $h = 0.004$ m.

In following tables, U stands for uniformly distributed, and UN stands for non-uniformly distributed.

Table 1 shows that regardless of whether the pores are uniformly or non-uniformly distributed, the fundamental frequency of FGM truncated shells decreases both with the increase of motion velocity V and the increase of material composition index N. For example, under uniform pore distribution, when the porosity α^* and material composition index N are taken as 0.05 and 0.2 respectively, the fundamental frequency decreases by 1.4% and 5.7% as the axial velocity increases from 0 m/s to 50 m/s and then to 100 m/s. When the porosity α^* and axial velocity V are taken as 0.05 and 50 m/s respectively, the vibration frequency decreases by 10.4%, 18.5%, and 24.9% respectively as the material composition index N increases from 0.2 to 0.5, 1.0, and 2.0. This is because the larger the material composition index N, the smaller proportion of ceramic materials. The elastic modulus of ceramics is larger than that of metals, so an increase in N inevitably leads to a decrease in overall stiffness, thereby a reduction of the natural frequency of truncated conical shells. Table 2 indicates that regardless of whether the pores are uniformly distributed or non-uniformly distributed, the fundamental frequency of the truncated shell decreases with the increase of the half cone angle but rises with the increase of the ceramic quality component. For example, under uniform pore distribution, when the poros-

ity α^* and ceramic quality component index N are taken as 0.05 and 0.1, the fundamental frequency decreases by 26.3%, 24.5%, and 22.2% respectively as the half cone angle gradually goes up from $\pi/6$ to $\pi/5$, $\pi/4$ and $\pi/3$. When the porosity α^* and half cone angle are taken as 0.05 and $\pi/6$, the fundamental frequency increases by 11.9% and 6.7% respectively as the ceramic quality component index N rises from 0.1 to 0.3 and then to 0.5.

Table 1

Dimensionless natural frequency f of FGM truncated conical shells under different axial motion velocities V and material composition indices N ($\gamma = \pi/4$, $W_c = 0.5$, $R_1/h = 100$, $L/R_1 = 1$)

V, m/s	α^*	N = 0.2		N = 0.5		N = 1.0		N = 2.0	
		U	NU	U	NU	U	NU	U	NU
0	0.05	0.3746	0.3727	0.3353	0.3352	0.3049	0.3059	0.2814	0.2831
	0.1	0.3725	0.3685	0.3334	0.3329	0.3030	0.3049	0.2796	0.2829
	0.2	0.3687	0.3602	0.3297	0.3282	0.2995	0.3027	0.2762	0.2825
50	0.05	0.3693	0.3674	0.3295	0.3293	0.2985	0.2995	0.2744	0.2761
	0.1	0.3673	0.3632	0.3275	0.3270	0.2966	0.2984	0.2725	0.2759
	0.2	0.3634	0.3547	0.3237	0.3222	0.2929	0.2962	0.2691	0.2755
100	0.05	0.3532	0.3511	0.3113	0.3111	0.2782	0.2793	0.2522	0.2541
	0.1	0.3510	0.3468	0.3091	0.3086	0.2762	0.2782	0.2502	0.2539
	0.2	0.3469	0.3378	0.3052	0.3036	0.2723	0.2758	0.2464	0.2535

Table 2

Dimensionless natural frequency f of FGM truncated conical shells under different ceramic material quality components and half cone angles (N = 1, R_1/h = 100, L/R_1 = 1, V = 50 m/s)

W_c	α^*	$\gamma = \pi/6$		$\gamma = \pi/5$		$\gamma = \pi/4$		$\gamma = \pi/3$	
		U	NU	U	NU	U	NU	U	NU
0.1	0.05	0.3385	0.3418	0.2496	0.2520	0.1884	0.1902	0.1466	0.1480
	0.1	0.3360	0.3424	0.2477	0.2525	0.1869	0.1906	0.1454	0.1483
	0.2	0.3313	0.3440	0.2443	0.2536	0.1843	0.1915	0.1434	0.1490
0.3	0.05	0.3788	0.3809	0.2797	0.2813	0.2115	0.2127	0.1650	0.1660
	0.1	0.3762	0.3804	0.2778	0.2808	0.2101	0.2124	0.1639	0.1657
	0.2	0.3714	0.3793	0.2742	0.2800	0.2074	0.2118	0.1618	0.1652
0.5	0.05	0.4040	0.4053	0.2985	0.2995	0.2260	0.2267	0.1765	0.1771
	0.1	0.4014	0.4039	0.2966	0.2984	0.2245	0.2259	0.1754	0.1765
	0.2	0.3965	0.4010	0.2929	0.2962	0.2218	0.2242	0.1732	0.1751

From the above two tables, it can be seen that the fundamental frequency of the truncated conical shell with uniformly distributed pores decreases with increasing porosity. The fundamental frequency of truncated conical shells with non-uniform distribution of pores increases with the increase of porosity when the ceramic material quality component $W_c = 0.1$, while the opposite is true when the ceramic material quality component W_c is greater than 0.1. The reason is the increase in internal pores of the shell weakens the overall stiffness while also reducing the mass. If the effect of pores on the overall stiffness is more significant than that on the mass, then the fundamental frequency decreases, and vice versa. In addition, it is found that compared to uniformly distributed pore shells, the natural vibration frequency of non-uniformly distributed pore shells is more sensitive to changes in porosity. When V = 50 m/s and the material composition index is 0.2 and 2.0, the fundamental frequency of uniformly distributed pore shells decreases by 1.60% and 1.93% with increasing porosity from 0.05 to 0.2, while the fundamental frequency of non-uniformly distributed pore shells decreases by 3.46% and 0.22%.

Table 3 shows the influence of geometric parameters (length to diameter ratio L/R_1, diameter to thickness ratio R_1/h) of truncated conical shells on the normalized fundamental frequency of FGM truncated conical shells with uniformly or non-uniformly distributed pores.

It can be seen from Table 3 that regardless of whether the pores are uniformly distributed or non-uniformly distributed, the increase either in the length to diameter ratio or in the diameter to thickness ratio both leads to a significant decrease in the fundamental frequency of the shell. For example, under uniform pore distribution, when the porosity α^* and diameter to thickness ratio R_1/h are taken as 0.05 and 100, the fundamental frequency of the shell decreases by 63.3% and 46.0% respectively as the length to diameter ratio increases from 0.25 to 0.5 and then to 1.0. When the porosity α^* and aspect ratio L/R_1 are taken as 0.05 and 0.25, the fundamental frequency of the shell decreases by 37.1% and 44.4% respectively as the aspect ratio increases from 100 to 120 and then to 150.

3.2.2. Dynamic response

In this subsection, the dynamic response of the mid-plane circumference at $s = (S_1+S_2)/2$ is taken as the example, and the effects of factors such as pore type, porosity, axial motion velocity, material composition index, ceramic material mass fraction, and geometric parameters on the dynamic response of axially moving porous FGM truncated conical shells are discussed. The uniformly distributed sudden load q = 0.1 kPa, and the thickness of the conical shell h = 0.01 m.

Fig. 4 shows the peak dynamic response of FGM truncated conical shells with either uniform or non-uniform pore distribution both increases with the porosity α* rising. When the porosity α* is taken as 0.05, 0.1, and 0.2 in

Table 3

Dimensionless natural frequency f of FGM truncated conical shells with uniform pore distribution under different aspect ratios ($\gamma = \pi/4$, $N = 1$, $W_c = 0.5$, $V = 60$ m/s)

R_1/h	α^*	L/R_1=0.25		L/R_1=0.5		L/R_1=1.0	
		U	NU	U	NU	U	NU
100	0.05	1.4922	1.4959	0.5473	0.5492	0.2956	0.2966
	0.1	1.4840	1.4909	0.5437	0.5472	0.2937	0.2955
	0.2	1.4690	1.4808	0.5369	0.5433	0.2900	0.2933
120	0.05	0.9383	0.9406	0.3386	0.3398	0.1782	0.1789
	0.1	0.9331	0.9375	0.3362	0.3385	0.1769	0.1782
	0.2	0.9235	0.9310	0.3318	0.3359	0.1745	0.1767
150	0.05	0.5217	0.5231	0.1763	0.1771	0.0815	0.0820
	0.1	0.5187	0.5213	0.1748	0.1763	0.0805	0.0814
	0.2	0.5130	0.5175	0.1721	0.1747	0.0788	0.0804

sequence, the peak dynamic deflection of shells with uniformly distributed pores is 4.2%, 10.1%, and 19.1% higher than those with non-uniform distribution, respectively. It can be seen that compared with non-uniform pore distribution shells, the peak dynamic deflection of shells with uniform pores varies more significantly with porosity. Fig. 5 shows that axial velocity has a significant impact on the dynamic deflection of FGM truncated conical shells, and the greater the velocity, the more significant reduction effect on their stiffness. Under uniform and non-uniform pore distribution, when the axial velocity V increases from 10m/s to 20 m/s, the peak dynamic deflection increases by 16.9% and 28.9%, respectively. When the speed changes from 20 m/s to 30 m/s, the peak dynamic deflection increases by 96.2% and 93.7%, respectively.

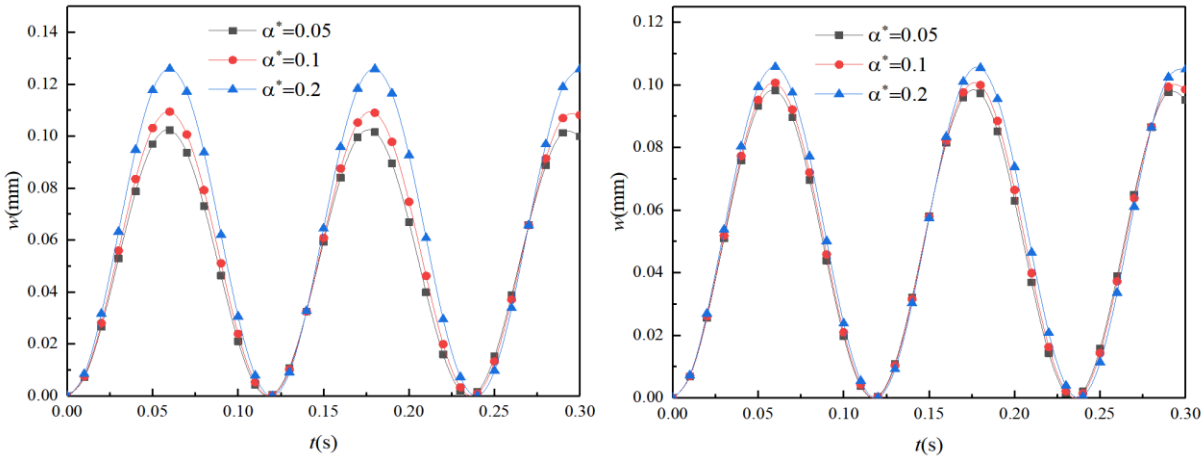

Fig. 4 Effect of porosity on the dynamic response of axially moving porous FGM truncated conical shells ($\gamma = \pi/3$, $N = 1$, $V = 15$ m/s, $Wc = 0.5$, $R_1/h = 100$, $L/R_1 = 2$): a – uniform pores, b – non-uniform pores

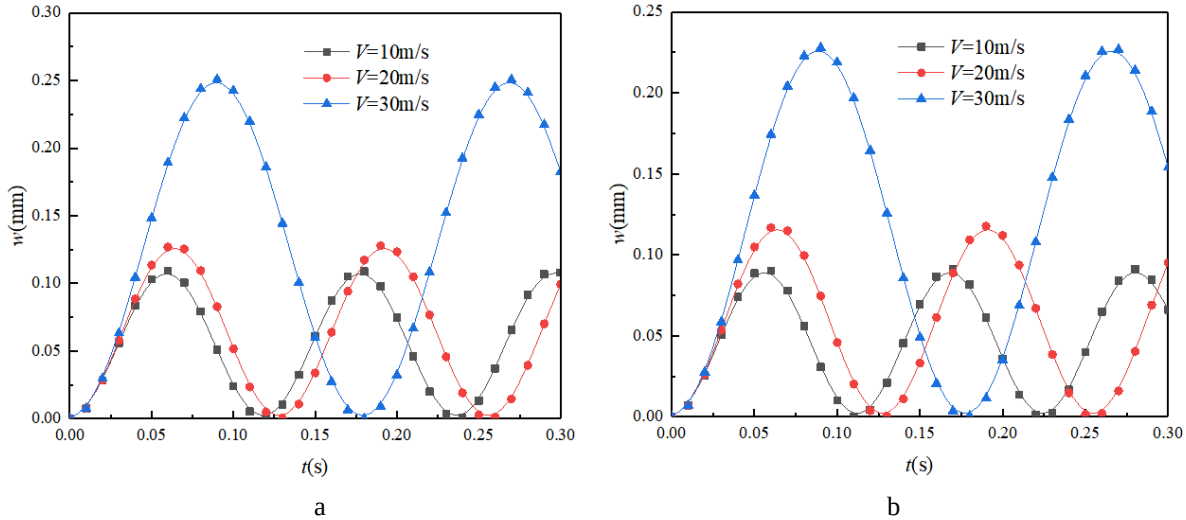

Fig. 5 Effect of axial velocity on the dynamic response of axially moving porous FGM truncated conical shells ($\gamma = \pi/3$, $N = 1$, $W_c = 0.5$, $a^* = 0.1$, $R_1/h = 100$, $L/R_1 = 2$): a – uniform pores, b – non-uniform pores

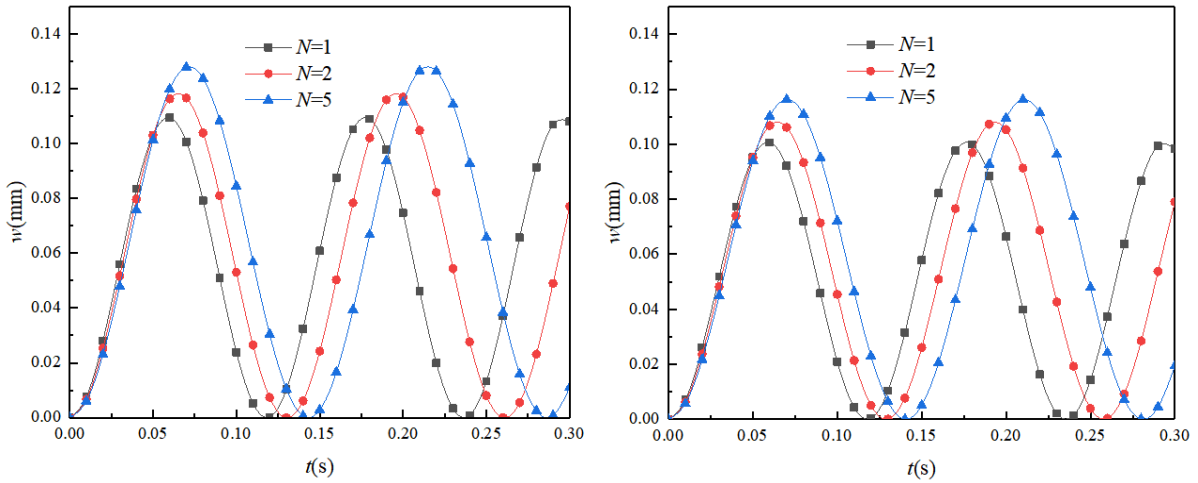

Fig. 6 Effect of material composition index on the dynamic response of axially moving porous FGM truncated conical shells ($\gamma = \pi/3$, V = 15 m/s, Wc = 0.5, a^* = 0.1, R_1/h = 100, L/R_1 = 2): a – uniform pores, b – non-uniform pores

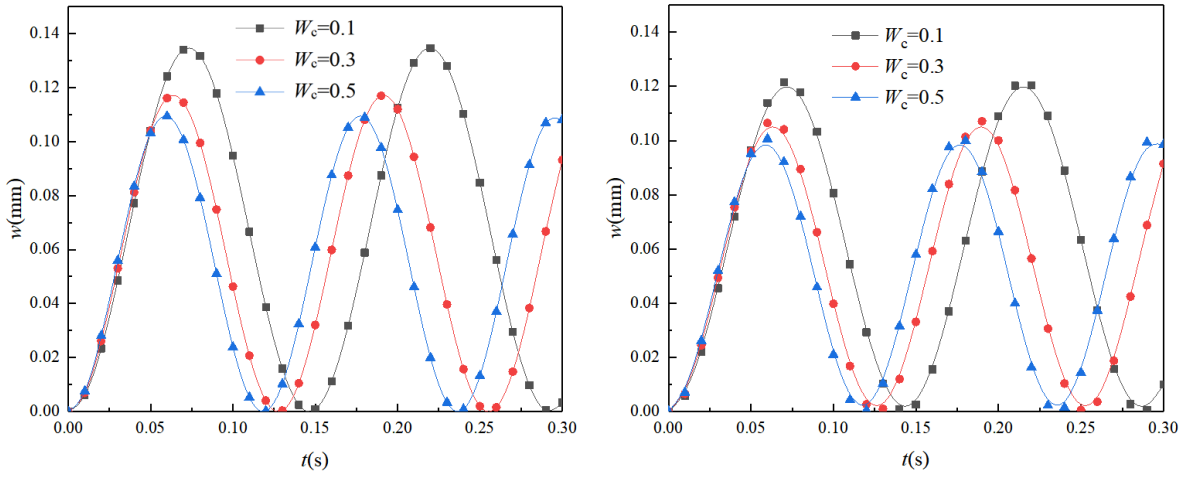

Fig. 7 Effect of the mass fraction of the ceramic material on the dynamic response of axially moving porous FGM truncated conical shells ($\gamma = \pi/3$, N = 1, V = 15 m/s, a^* = 0.1, R_1/h = 100, L/R_1 =2): a – uniform pores, b – non-uniform pores

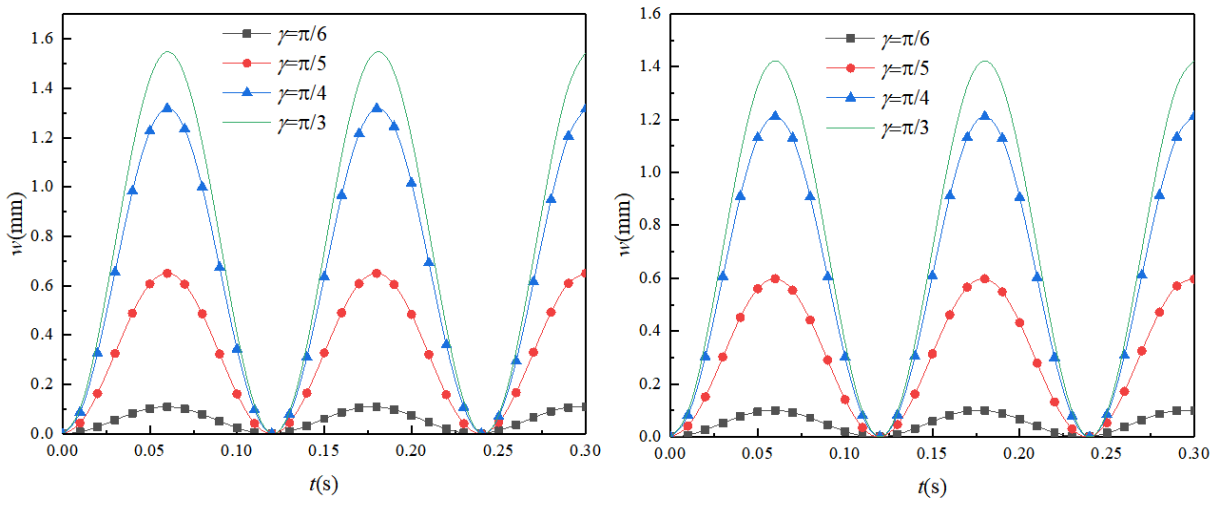

Fig. 8 Effect of half cone angle on the dynamic response of axially moving porous FGM truncated conical shells (N = 1, V = 15 m/s, W_c = 0.5, a^* = 0.1, R_1/h = 100, L/R_1 = 2): a – uniform pores, b – non-uniform pores

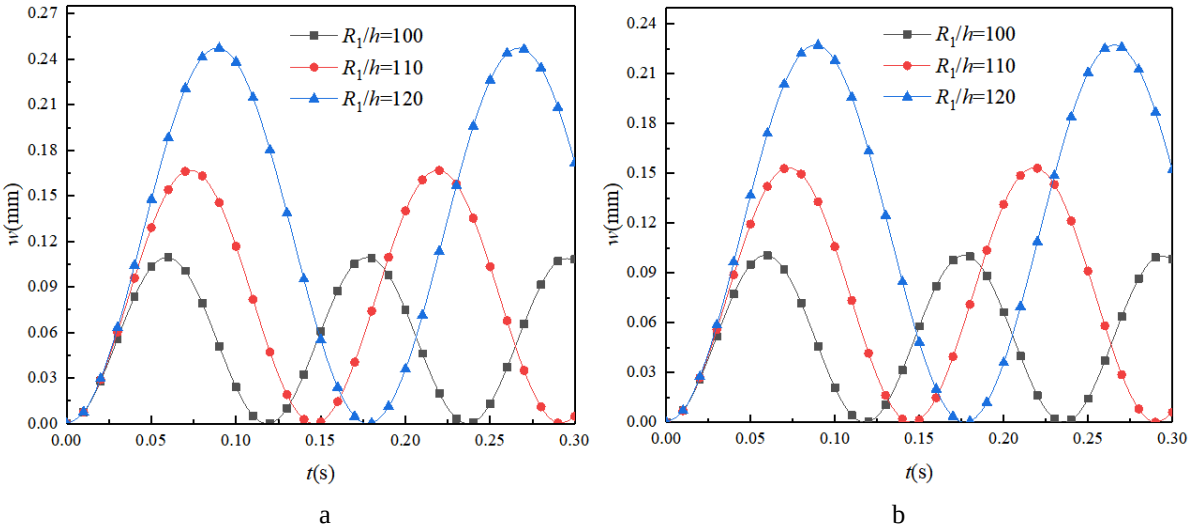

Fig. 9 Effect of diameter thickness ratio on the dynamic response of axially moving porous FGM truncated conical shells ($\gamma = \pi/3$, $N = 1$, $V = 15$ m/s, $W_c = 0.5$, $a^* = 0.1$, $L/R_1 = 2$): a – uniform pores, b – non-uniform pores

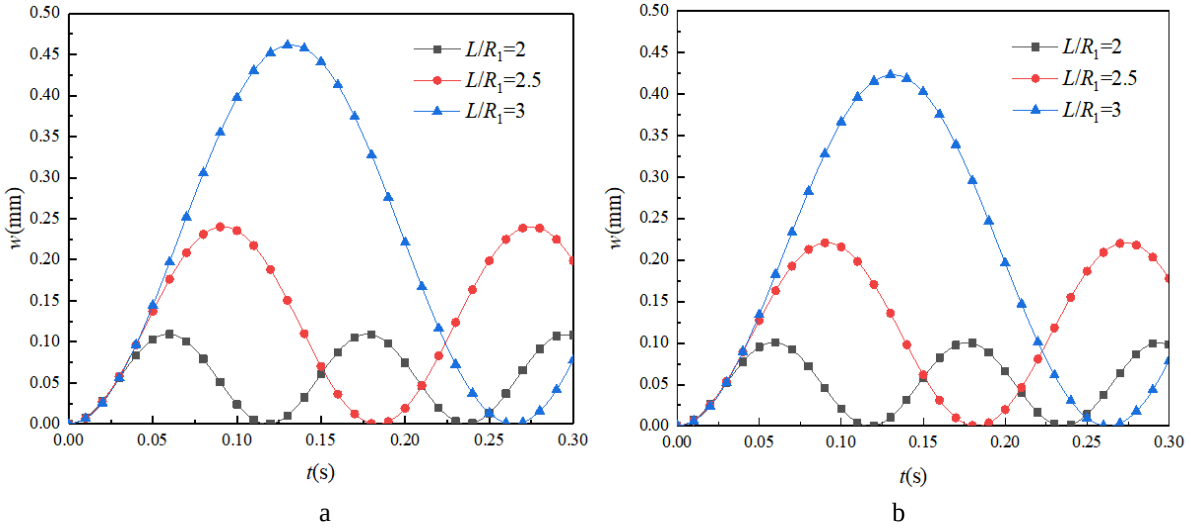

Fig. 10 Effect of aspect ratio on the dynamic response of axially moving porous FGM truncated conical shells ($\gamma = \pi/3$, $N = 1$, $V = 15$ m/s, $W_c = 0.5$, $a^* = 0.1$, R_1/h =100): a – uniform pores, b – non-uniform pores

From Figs. 6 and 7, it can be seen that the peak dynamic deflection of shells rises with the increase of material composition index and goes down with the increase of ceramic material mass composition.

Fig. 8 shows that the half cone angle has a significant impact on the dynamic deflection of shells containing either uniformly distributed or non-uniformly distributed pores. When the pores are uniformly distributed, the peak dynamic deflection of the shell decreases by 83.2% as the half cone angle increases from $\pi/6$ to $\pi/3$.

Fig. 9 shows that an increase in the diameter to thickness ratio causes the truncated shell to become relatively thinner, thereby reducing the overall stiffness of the shell. When the diameter to thickness ratio R_1/h increases from 100 to 110, and then to 120, the dynamic deflection amplitude of the shell with uniformly distributed pores increases by 52.4% and 48.3%, successively.

From Fig. 10, it is found that when the length to diameter ratio L/R1 rises from 2 to 2.5 and 3, the dynamic deflection amplitude of the shell with uniformly distributed pores increases by 119.5% and 92.0% successively. This indicates that an increase in the length to diameter ratio leads to a relatively longer length of the truncated shell, resulting in a significant decrease in its effective stiffness.

4. Conclusions

Based on an improved mixed law model and classical thin shell theory, this article establishes the vibration equation of axially moving FGM truncated conical shells with uniform or non-uniform pores, and the Galerkin integration method is used to calculate their natural frequency and dynamic response under simply supported boundary conditions at both ends. The effects of axial motion velocity, ceramic material mass fraction, porosity, pore type, geometric parameters, and other factors on the vibration frequency and dynamic response of shells are specifically discussed, and from the results following conclusions can be drawn.

1. The increase in axial motion speed reduces the effective stiffness of the shell, resulting in a decrease in the natural frequency and an increase in dynamic response.

2. The influence of pores on the natural frequency of shells is constrained by various factors, and the effects

of porosity size and pore distribution type can neither be ignored. The increase in porosity increases the dynamic response of the shell, and under the same conditions, the dynamic response of the shell with uniformly distributed pores is greater than that with non-uniformly distributed pores.

3. The vibration frequency of the shell continuously increases with the rise of the ceramic material quality component, and gradually decreases with the increase of the material component index. And for shell's dynamic response, these two factors both have the opposite effect.

4. The vibration frequency of the shell goes down significantly with the increase in either half cone angle, diameter to thickness ratio, or length to diameter ratio, and results in a rise of dynamic response. Therefore, appropriately reducing the half cone angle, increasing the thickness of the shell, or shortening the length of the generatrix can effectively improve the overall stiffness of the conical shell.

Acknowledgments

This work was supported by National Natural Science Foundation of China (No. 12162010) and Guangxi Natural Science Foundation (No. 2021GXNSFAA220087).

References

1. **Awrejcewicz, J. Krysko, A.V., Pavlov, S.P., Zhigalov, M.V., Krysko, V.A.** 2017. Stability of the Size-Dependent and Functionally Graded Curvilinear Timoshenko Beams, ASME. J. Comput. Nonlinear Dynam. 12(4): 041018. https://doi.org/10.1115/1.4035668.
2. **Mahesh, V.** 2022. Nonlinear damping of auxetic sandwich plates with functionally graded magneto-electro-elastic facings under multiphysics loads and electromagnetic circuits, Composite Structures 290: 115523. https://doi.org/10.1016/j.compstruct.2022.115523.
3. **Avey, M.; Fantuzzi, N.; Sofiyev, A.H**. 2022. Mathematical modeling and analytical solution of thermoelastic stability problem of functionally graded nanocomposite cylinders within different theories, Mathematics 10: 1081. https://doi.org/10.3390/math10071081.
4. **Zhang, J.; Li, S**. 2013. Free Vibration of Functionally Graded Truncated Conical Shells Using the GDQ Method, Mechanics of Advanced Materials and Structures 20: 61 - 73. http://dx.doi.org/10.1080/15376494.2011.581415.
5. **Sofiyev, A. H**. 2015. On the vibration and stability of shear deformable FGM truncated conical shells subjected to an axial load, Composites Part B-engineering 80: 53-62. http://dx.doi.org/10.1016/j.compositesb.2015.05.032
6. **Sofiyev, A. H.** 2016. Thermoelastic stability of freely supported functionally graded conical shells within the shear deformation theory, Compos. Struct. 152: 74-84. https://dx.doi.org/10.1016/j.compstruct.2016.05.027.
7. **Sofiyev, A. H.; Osmancelebioglu, E**. 2017. The free vibration of sandwich truncated conical shells containing functionally graded layers within the shear deformation theory, Composites Part B-engineering 120: 197-211. http://dx.doi.org/10.1016/j.compositesb.2017.03.054
8. **Sofiyev, A. H**. 2019. Review of research on the vibration and buckling of the FGM conical shells, Composite Structures 211: 301-317. https://doi.org/10.1016/j.compstruct.2018.12.047.
9. **Abolhassanpour, H.; Shahgholi, M.; Ashenai Ghasemi, F.; Mohamadi, A**. 2021. Nonlinear vibration analysis of an axially moving thin-walled conical shell, International Journal of Non-linear Mechanics, 134: 103747. http://dx.doi.org/10.1016/j.ijnonlinmec.2021.103747.
10. **Nezhadi, A.; Rahman, R.A.; Ayob, A., Fard, K.M.** 2012. Free and Forced Vibrations of FGM Conical Shell Under Impulse Loads, Research Journal of Applied Sciences, Engineering and Technology 4(20): 4055-4065.
11. **Rahmani, M.; Mohammadi, Y.; Kakavand, F.; Raeisifard, H**. 2020. Vibration Analysis of Different Types of Porous FG Conical Sandwich Shells in Various Thermal Surroundings, Applied and Computational Mechanics 6: 416-432. http://dx.doi.org/10.22055/JACM.2019.29442.1598.
12. **Cong, P.H.; Chien, T.M.; Khoa, N.D.; Duc, N.D**. 2018. Nonlinear thermomechanical buckling and post-buckling response of porous FGM plates using Reddy's HSDT, Aerospace Science and Technology 77: 419-428. http://dx.doi.org/10.1016/J.AST.2018.03.020.
13. **Huang, X.; Lei, D. X.; Wei, G.; Zhong, D**. 2019. Nonlinear free and forced vibrations of porous sigmoid functionally graded plates on nonlinear elastic foundations, Composite Structures 228: 111326. http://dx.doi.org/10.1016/j.compstruct.2019.111326.
14. **Allahkarami, F.; Saryazdi, M. G.; Tohidi, H.** 2020. Dynamic buckling analysis of bi-directional functionally graded porous truncated conical shell with different boundary conditions, Composite Structures 252: 112680. http://dx.doi.org/10.1016/j.compstruct.2020.112680.
15. **Wang, Y. Q.; Wan, Y. H.; Zhang, Y. F**. 2017. Vibrations of longitudinally traveling functionally graded material plates with porosities, European Journal of Mechanics A-solids 66: 55-68. http://dx.doi.org/10.1016/j.euromechsol.2017.06.006.
16. **Phung-Van, P.; Thai, C. H.; Nguyen-Xuan, H.; Abdel Wahab, M**. 2019. Porosity-dependent nonlinear transient responses of functionally graded nanoplates using isogeometric analysis, Composites Part B: Engineering 164: 215-225. http://dx.doi.org/10.1016/j.compositesb.2018.11.036
17. **Fu, T.; Wu, X., Xiao; Z.M.; Chen, Z**. 2021. Dynamic instability analysis of porous FGM conical shells subjected to parametric excitation in thermal environment within FSDT, Thin-walled Structures 158: 107202. http://dx.doi.org/10.1016/j.tws.2020.107202.
18. **Mahesh, V; Mahesh, V.; Ponnusami, S.A.** 2023. FEM-ANN approach to predict nonlinear pyro-coupled deflection of sandwich plates with agglomerated porous nanocomposite core and piezo-magneto-elastic facings in thermal environment, Mechanics of Advanced Materials and Structures. https://doi.org/10.1080/15376494.2023.2201927.
19. **Mahesh, V.** 2021. Porosity effect on the energy har-

vesting behaviour of functionally graded magneto-electro-elastic fibre-reinforced composite beam, Eur. Phys. J. Plus. 137(1): 48. https://doi.org/10.1140/epjp/s13360-021-02235-9.

20. **Mahesh, V.** 2022. Porosity effect on the nonlinear deflection of functionally graded magneto-electro-elastic smart shells under combined loading, Mechanics of Advanced Materials and Structures 29(19): 2707-2725. https://doi.org/10.1080/15376494.2021.1875086.
21. **Hong, M.; Lee, U.** 2015. Dynamics of a functionally graded material axial bar: Spectral element modeling and analysis, Composites Part B-engineering, 69: 427-434. http://dx.doi.org/10.1016/j.compositesb.2014.10.022.
22. **Shen, J.P.; Wang, P.; Gan, W.T.; Li, C.; Li, C.** 2020. Stability of Vibrating Functionally Graded Nanoplates with Axial Motion Based on the Nonlocal Strain Gradient Theory, International Journal of Structural Stability and Dynamics 20(8): 2050088. http://dx.doi.org/10.1142/S0219455420500881.
23. **Yan, T.; Yang, T.; Chen, L.** 2020. Direct Multiscale Analysis of Stability of an Axially Moving Functionally Graded Beam with Time-Dependent Velocity, Acta Mechanica Solida Sinica 33(2): 150-163. http://dx.doi.org/10.1007/s10338-019-00140-4.
24. **Allahkarami, F.; Saryazdi, M. G.; Tohidi, H.** 2020. Dynamic buckling analysis of bidirectional functionally graded porous truncated conical shell with different boundary conditions, Composite Structures 252: 112680. http://dx.doi.org/10.1016/j.compstruct.2020.112680.
25. **Sofiyev, A.H.** 2010. The buckling of FGM truncated conical shells subjected to axial compressive load and resting on Winkler-Pasternak foundations, International Journal of Pressure Vessels and Piping 87(12): 753-761. http://dx.doi.org/10.1016/j.ijpvp.2010.08.012.
26. **Chan, D.Q.; Anh, V.T.T.; Duc, N.D**. 2019. Vibration and nonlinear dynamic response of eccentrically stiffened functionally graded composite truncated conical shells surrounded by an elastic medium in thermal environments, Acta Mechanica 230(1): 157-178. http://dx.doi.org/10.1007/s00707-018-2282-4.

Appendix A

$A_{ij}^{*}(1,2,6)$ and $B_{ij}^{*}(1,2,6)$ are constants and are given below:

$$A_{11}^{*}=\frac{A_{11}}{\Delta},\ A_{12}^{*}=\frac{-A_{21}}{\Delta},\ A_{21}^{*}=\frac{-A_{12}}{\Delta},\ A_{22}^{*}=\frac{A_{22}}{\Delta},$$

$$A_{66}^{*}=\frac{1}{A_{66}},\ B_{11}^{*}=\frac{B_{11}A_{21}-A_{11}B_{21}}{\Delta},$$

$$B_{12}^{*}=\frac{B_{12}A_{21}-A_{11}B_{22}}{\Delta},\ B_{21}^{*}=\frac{A_{12}B_{21}-B_{11}A_{22}}{\Delta},$$

$$B_{22}^{*}=\frac{A_{12}B_{22}-B_{12}A_{22}}{\Delta},\ B_{66}^{*}=-\frac{B_{66}}{A_{66}}.$$

Appendix B

$C_{ij}^{*}(1,2,6)$ and $D_{ij}^{*}(1,2,6)$ are constants and are given below:

$$C_{11}^{*}=\left(B_{11}A_{21}^{*}+B_{12}A_{11}^{*}\right),\ C_{12}^{*}=\left(B_{11}A_{22}^{*}+B_{12}A_{12}^{*}\right),$$

$$C_{21}^{*}=\left(B_{21}A_{21}^{*}+B_{22}A_{11}^{*}\right),\ C_{22}^{*}=\left(B_{21}A_{22}^{*}+B_{22}A_{12}^{*}\right),$$

$$C_{66}^{*}=B_{66}A_{66}^{*},\ D_{11}^{*}=\left(B_{11}B_{21}^{*}+B_{12}B_{11}^{*}+D_{11}\right),$$

$$D_{12}^{*}=\left(B_{11}B_{22}^{*}+B_{12}B_{12}^{*}+D_{12}\right),$$

$$D_{21}^{*}=\left(B_{21}B_{21}^{*}+B_{22}B_{11}^{*}+D_{21}\right),$$

$$D_{22}^{*}=\left(B_{21}B_{22}^{*}+B_{22}B_{12}^{*}+D_{22}\right),\ D_{66}^{*}=\left(D_{66}+B_{66}B_{66}^{*}\right).$$

Appendix C

$g_{ijk}(1,2,\ldots,8)$ are parameters and are given below:

$$g_{111}=\frac{-\left(2C_{22}^{*}-2C_{11}^{*}+2C_{21}^{*}-2C_{12}^{*}\right)}{S_1^3},$$

$$g_{112}=\frac{-\left(C_{22}^{*}-5C_{11}^{*}+3C_{21}^{*}-3C_{12}^{*}\right)}{S_1^3},$$

$$g_{113}=\frac{-\left(-4C_{11}^{*}+C_{21}^{*}-C_{12}^{*}\right)}{S_1^3},$$

$$g_{114}=\frac{C_{11}^{*}}{S_1^3},\ g_{115}=\frac{-\left(-2C_{22}^{*}+2C_{66}^{*}-2C_{21}^{*}\right)}{S_1^3},$$

$$g_{116}=\frac{-\left(-3C_{21}^{*}-C_{12}^{*}+4C_{66}^{*}\right)}{S_1^3},\ g_{117}=\frac{-\left(-C_{21}^{*}-C_{12}^{*}+2C_{66}^{*}\right)}{S_1^3},$$

$$g_{118}=\frac{C_{22}^{*}}{S_1^3},\ g_{121}=\frac{-\left(-2D_{11}^{*}-2D_{21}^{*}+2D_{12}^{*}+2D_{22}^{*}\right)}{S_1^3},$$

$$g_{122}=\frac{-\left(5D_{11}^{*}+3D_{21}^{*}-3D_{12}^{*}-D_{22}^{*}\right)}{S_1^3},\ g_{124}=\frac{-D_{11}^{*}}{S_1^3},$$

$$g_{125}=\frac{-\left(2D_{12}^{*}+2D_{66}^{*}+2D_{22}^{*}\right)}{S_1^3},$$

$$g_{126}=\frac{-\left(-D_{21}^{*}-3D_{12}^{*}-4D_{66}^{*}\right)}{S_1^3},$$

$$g_{127}=\frac{-\left(D_{21}^{*}+D_{12}^{*}+2D_{66}^{*}\right)}{S_1^3},\ g_{128}=\frac{-D_{22}^{*}}{S_1^3},$$

$$g_{211}=\frac{2\left(A_{11}^{*}+A_{12}^{*}-A_{21}^{*}-A_{22}^{*}\right)}{S_1^4},$$

$$g_{212}=\frac{\left(5A_{11}^{*}+3A_{12}^{*}-3A_{21}^{*}-A_{22}^{*}\right)}{S_1^4},\ g_{213}=\frac{\left(4A_{11}^{*}+A_{12}^{*}-A_{21}^{*}\right)}{S_1^4},$$

$$g_{214}=\frac{A_{11}^{*}}{S_1^4},\ g_{215}=\frac{\left(2A_{21}^{*}+2A_{22}^{*}+A_{66}^{*}\right)}{S_1^4},\ g_{216}=\frac{A_{22}^{*}}{S_1^4},$$

$$g_{217}=\frac{\left(A_{12}^{*}+3A_{21}^{*}+2A_{66}^{*}\right)}{S_1^4},\ g_{218}=\frac{\left(A_{12}^{*}+A_{21}^{*}+A_{66}^{*}\right)}{S_1^4},$$

$$g_{221}=\frac{\left(2B_{11}^{*}-2B_{12}^{*}+2B_{21}^{*}-2B_{22}^{*}\right)}{S_1^4},$$

$$g_{222}=\frac{\left(B_{22}^{*}-5B_{11}^{*}+3B_{12}^{*}-3B_{21}^{*}\right)}{S_1^4},$$

$$g_{223}=\frac{\left(-B_{12}^{*}+B_{21}^{*}+4B_{11}^{*}\right)}{S_1^4},\ g_{224}=\frac{-B_{11}^{*}}{S_1^4},$$

$$g_{225}=\frac{\left(-2B_{12}^{*}-2B_{22}^{*}+B_{66}^{*}\right)}{S_1^4},$$

$$g_{226}=\frac{-B_{22}^{*}}{S_1^4},\ g_{227}=\frac{\left(-2B_{66}^{*}+B_{21}^{*}+3B_{12}^{*}\right)}{S_1^4},$$

$$g_{228}=\frac{\left(B_{66}^{*}-B_{21}^{*}-B_{12}^{*}\right)}{S_1^4}.$$

Appendix D

$a_{ij}(1,2,\ldots,4)$ are parameters and are given below:

$$a_{11}=-\frac{1}{2}m_1\begin{pmatrix}m_1^2g_{213}-4m_1^2g_{214}+n_1^2g_{217}-\\-2n_1^2g_{218}-g_{211}+2g_{212}-3g_{213}+4g_{214}\end{pmatrix},$$

$$a_{12}=\frac{1}{2}\begin{pmatrix}m_1^4g_{214}+m_1^2n_1^2g_{218}+n_1^4g_{216}-m_1^2g_{212}+\\+3m_1^2g_{213}-6m_1^2g_{214}+n_1^2g_{217}-n_1^2g_{218}-\\-g_{211}+g_{212}-g_{213}+g_{214}\end{pmatrix},$$

$$a_{13}=\frac{1}{2}m_1\begin{pmatrix}ln^3(e)\left(4g_{224}+3g_{223}\right)-\\-2ln(e)\left(2m_1^2g_{224}-n_1^2g_{228}\right)-\\-m_1^2g_{223}-n_1^2g_{227}+2ln(e)g_{222}+g_{221}\end{pmatrix},$$

$$a_{14}=\frac{1}{2}\begin{pmatrix}ln^4(e)g_{224}-6ln^2(e)m_1^2g_{224}-ln^2(e)n_1^2g_{228}+\\+m_1^4g_{224}+m_1^2n_1^2g_{228}+n_1^4g_{226}+ln^3(e)g_{223}-\\-3ln(e)m_1^2g_{223}-ln(e)n_1^2g_{227}+ln^2(e)g_{222}-\\-m_1^2g_{222}-n_1^2g_{225}+ln(e)g_{221}\end{pmatrix},$$

$$a_{21}=-\frac{1}{2}m_1\left(m_1^2g_{213}+n_1^2g_{217}-g_{211}\right),$$

$$a_{22}=\frac{1}{2}\left(m_1^4g_{214}+m_1^2n_1^2g_{218}+n_1^4g_{216}-m_1^2g_{212}\right),$$

$$a_{23}=\frac{m_1\cos(\gamma)\left(2ln(e)-1\right)}{2S_1^3},$$

$$a_{24}=\frac{e^{-2x}\cos(\gamma)\left(ln^2(e)-m_1^2-ln(e)\right)}{2S_1^3}.$$

W. Xiao, S. Liu, X. Huang, X. Wu, X. Yuan

VIBRATION ANALYSIS OF POROUS FUNCTIONALLY GRADED MATERIAL TRUNCATED CONICAL SHELLS IN AXIAL MOTION

S u m m a r y

In this study, a vibration equation for axially moving truncated conical thin shells made of functionally gradient materials with uniformly and non-uniformly distributed pores has been established based on classical thin shell theory. The free vibration and dynamic response solutions are obtained using the Galerkin method. The effects of axial velocity, half cone angle, ceramic material mass composition, material component index, and internal porosity on the free vibration and dynamic response of mentioned shells were analyzed and discussed. The results show that the increase of axial velocity, half cone angle, and material composition index all decrease the natural frequency of the truncated conical shell but amplify its dynamic response, and the rise of the mass fraction of the ceramic material increases the natural frequency of the truncated conical shell but reduces the dynamic response. The results also demonstrate that compared with non-uniformly distributed pores, the effects of uniformly distributed pores on the shells' dynamic responses are more evident under axial motion.

Keywords: functionally graded material, truncated conical shell, pore, axial motion, vibration.

Received July 8, 2023
Accepted April 15, 2024